Supplemental Material: "On the Impact of Solvation on a Au/TiO_2 Nanocatalyst in Contact with Water"

Matteo Farnesi Camellone and Dominik Marx

Lehrstuhl für Theoretische Chemie, Ruhr–Universität Bochum, 44780 Bochum, Germany

The $TiO_2(110)$ surfaces were modeled by four $O - Ti_2O_2 - O$ trilayer (4x2) supercell slabs separated by more than 15 Å of vacuum space normal to the surface. The bottom of the slab was passivated with pseudohydrogen atoms of nuclear charge +4/3 and +2/3 in order to achieve well–converged results. This is our so–called "standard setup" which has been previously [1] carefully constructed and benchmarked by performing extensive tests on the convergence of surface energies as well as hydrogen and water adsorption energies, with respect to both the number of relaxed outermost trilayers and the thickness of the slab itself (see tables and graphs in Ref. 1 for detailed comparisons). The gradient–corrected Perdew-Burke-Ernzerhof (PBE) [2] density functional was employed and has been extensively validated to describe accurately interactions of molecules with titania [1]. The spin–polarized Kohn-Sham equations were solved in the plane wave / pseudopotential framework using Vanderbilt's ultrasoft pseudopotentials [3] with a cutoff of 25 Ry using the Γ–point. The Ti pseudopotential was constructed from an ionic $3d^1 4s^2$ configuration and the $3s$ and $3p$ semicore electrons were treated as full valence states. The lowest trilayer atoms were constrained to their equilibrium positions, while all other atoms were free to move.

It is well established that adding a Hubbard U term acting on the Ti–$3d$ orbitals greatly improves the quality of LDA or GGAs in describing the electronic structure of both oxidized and reduced titania surfaces [4–12]. Following our previous work [12], we used a self–consistent linear response formalism [14, 15] to compute the Hubbard term, which turns out to be U = 4.2 eV for this particular setup; the occupations of the d orbitals were calculated using atomic–like wave function projectors.

The static optimizations for the different $TiO_2(110)$ surface structures were carried out using the `Quantum Espresso` [16] code. All structures were relaxed by minimizing the atomic forces, where convergence was assumed to have been achieved when the maximum component of the residual forces on the ions was less than 0.02 eV/Å. All *ab initio* molecular dynamics (AIMD) simulations [17] were carried out using the same spin–polarized PBE+U approach, together with the Car–Parrinello propagation scheme [18], using a fictitious orbital mass of 500 a.u. and a AIMD time step of 0.12 fs. The canonical ensemble was employed with a target temperature of 450 K and established with a Nosé-Hoover thermostat chain. Our in-house modified version of the `CPMD` [19] code was used for carrying out all AIMD simulations.

In modeling gold nanoparticles supported by this $TiO_2(110)$ surface model, we have de-

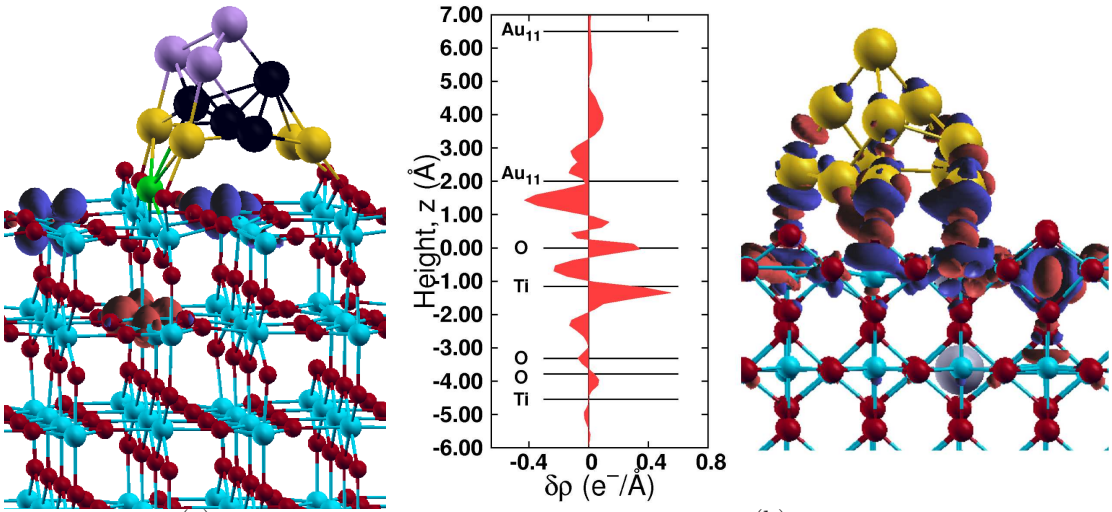

FIG. 1: (a) Ball and stick model of the Au_{11} nanocluster pinned by an F–center on the $TiO_2(110)$ oxide surface. Red, big blue and small blue spheres are O, Ti, and H, respectively, whereas the surface O vacancy is shown in green. Blue and red isosurfaces represent the spin density (at 0.005 $e/Å^3$) (b) Charge density difference $\Delta\rho(\vec{r})$ of the $Au_{11}/TiO_2(110)$ catalyst integrated in planes perpendicular to the surface and plotted as a function of the height from the surface ($\Delta\rho(z)$), and 3D plot of the bonding charge $\Delta\rho(\vec{r})$. Electron depletion and accumulation are depicted by blue and red areas, respectively, and plotted at the value of $\pm$ 0.02 $|e|/Å^3$.

posited Au_{11} clusters on the $TiO_2(110)$ surface where an F–center created by a surface O vacancy acts as anchoring site for initial Au nucleation; see Ref. 13 for previous work on the properties of F–centers in relation to the adsorption of molecules and gold on $TiO_2(110)$. Figure 1(a) shows the resulting $Au/TiO_2(110)$ nanocatalyst employed in the simulations. The binding of the Au_{11} cluster on this reduced oxide support entails a strong charge rearrangement at the gold/oxide contact, the adsorption energy being -2.19 eV.

In the case of an isolated O vacancy on the stoichiometric $TiO_2(110)$ surface, the charge neutrality is maintained by the presence of two Ti^{3+} ions (F–center). The spin density analysis presented in Fig. 1(a) reveals that the Au_{11} cluster, once adsorbed, leaves a reduced $TiO_2(110)$ substrate with three Ti^{3+} ions. As depicted in Fig. 1(a), two of the three excess electrons are trapped at two first layers Ti, whereas the third is localized on a second layer site. Finite temperature dynamics does not modify the degree of reduction of the oxide support, which entails the presence of three Ti^{3+} ions along the full trajectory. This is

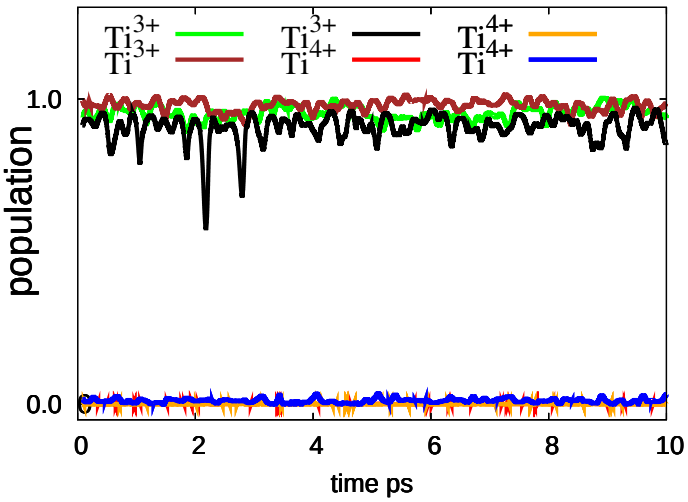

FIG. 2: Dynamics of the fractional occupation of selected Ti d orbitals during the PBE+U simulation of the $Au_{11}/TiO_2(110)$-H_2O interface. Populations of about 1 and 0 correspond to Ti^{3+} and Ti^{4+} charge states, respectively. The three excess electrons (Ti^{3+}) in the substrate are always trapped at the same Ti sites along the full trajectory. The same behavior is observed in the reference gas phase simulation.

true in the liquid phase (see below) as well as in the gas phase. Moreover, as shown in Fig. 2, the excess electrons populating the oxide substrate remain always localized on the same Ti sites. No charge transfer is observed between Ti sites of the reduced $TiO_2(110)$ surface. The bonding charge analysis of Fig. 1(b) reveals that 0.4 $|e|$ are transferred from the metal cluster to the oxide, leading to the formation of a slightly positively charged $Au_{11}^{\delta+}$ cluster supported on a reduced $TiO_2(110)$ oxide surface. This magnitude of charge transfer is obtained by integrating the bonding charge on planes parallel to the surface from the middle of the vacuum region to the middle of the bottom Au–O bond lengths, i.e. using

$$\int\int \sum_{i=-,+} \Delta\rho_i dxdy \ . \tag{1}$$

In order to create the solvated system being the subject of study in the associated manuscript, i.e. the $Au_{11}/TiO_2(110)$–water interface, the space between the $Au_{11}/TiO_2(110)$ slabs has been fully filled using 53 H_2O water molecules. The number of water molecules has been chosen to adjust the effective density of water to the ambient density of water. In Table I we report the time averaged Löwdin charge values of each Au atom of the $Au_{11}/TiO_2(110)$

TABLE I: Time averaged Löwdin charges of each Au atom. The last three columns show to which layer(s) of the gold cluster the Au atoms belong.

	Löwdin charge	Löwdin charge	layer		
	liquid phase	gas phase	top	middle	bottom
Au	11.02	11.0	x		
Au	11.03	10.97	x		
Au	11.04/11.23*	10.93	x		
Au	11.20	11.25		x	
Au	11.26	11.08		x	
Au	11.21	11.06		x	
Au	11.20	11.07		x	
Au	11.04	10.98			x
Au	11.06	11.06			x
Au	11.16	11.02			x
Au	11.23	10.97			x

* The two charge values correspond to the time average obtained before and after the jumping event around 6 ps (see associated manuscript).

nanocatalyst in contact with liquid. The charge mean values of top and middle Au atoms are ~ 11.0 and ~ 11.2 $|e|$, respectively. This implies that in the liquid phase top and middle gold atoms are stabilized at distinct charge states.

We now turn to describe the change in the structure and "morphology" of the gold supported nanocluster in both the liquid and gas phase situations. As discussed, we have performed two sets of simulations. In one simulation we have employed as starting configuration the $Au_{11}/TiO_2(110)$ nanocatalyst solvated with water, while in the other simulation the $Au_{11}/TiO_2(110)$ in the gas phase has been used as initial structure. Then, a series of snapshots of the $Au_{11}/TiO_2(110)$–water interface has been selected. The water molecules have been removed from the combined systems and the substrates have been quenched to $T = 0$ K. The Löwdin charges of Au atoms before and after the quenching are plotted in the left panels (a) and (c) of Fig. 3. Note that Fig. 3(a) differs from Fig. 1(b) of the associated

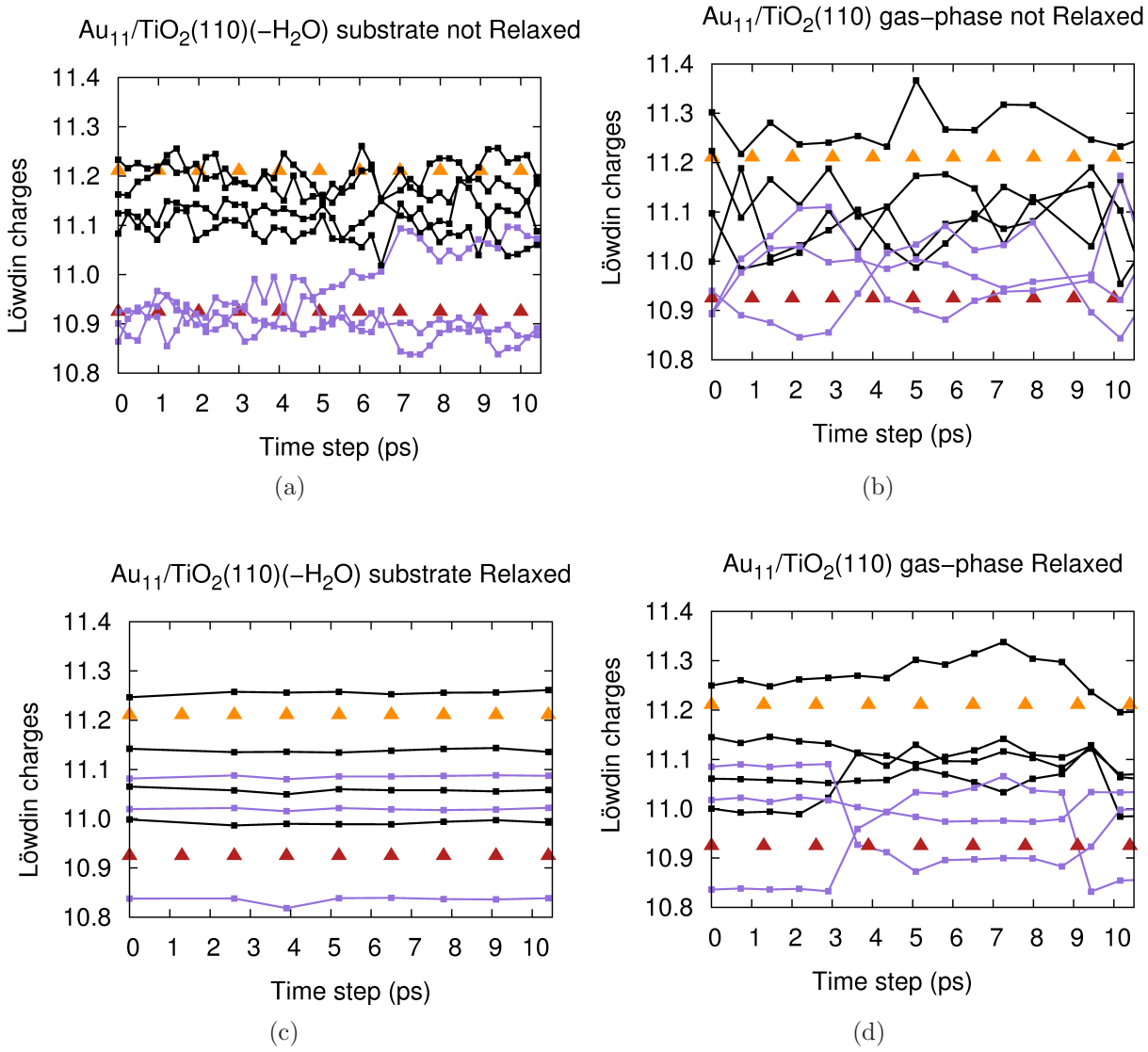

FIG. 3: Evolution of the Löwdin charges of top (violet lines) and middle (black lines) Au atoms of selected snapshots of the supported gold nanocluster as a function of the simulation time. Left panel: Löwdin charges of Au atoms of the $Au_{11}/TiO_2(110)$–water interface before (a) and after (c) quenching. Here, the charges have been computed after removing all H_2O molecules from the combined $Au_{11}/TiO_2(110)$–water system. Right panel: Löwdin charges of Au atoms of $Au_{11}/TiO_2(110)$ in contact with a gas phase before (b) and after (d) quenching.

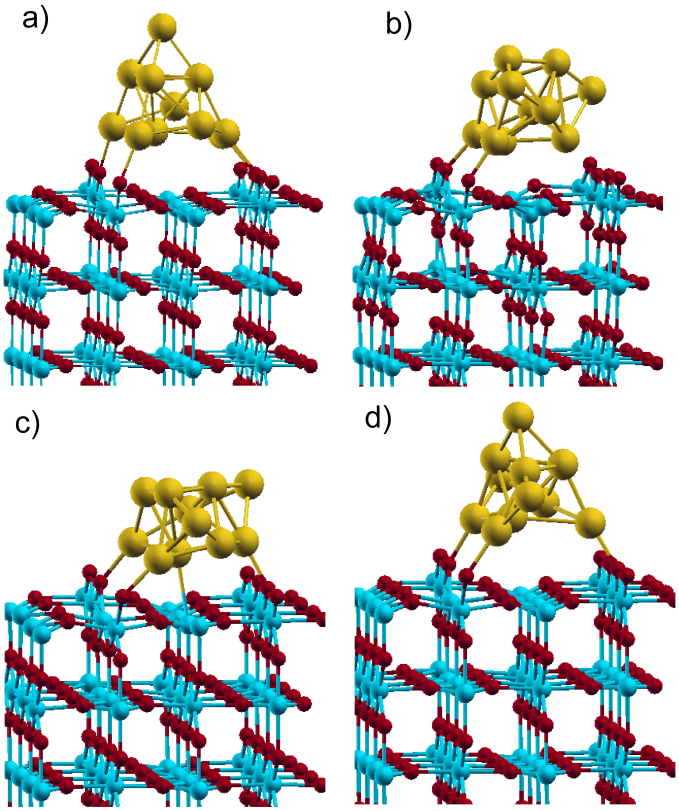

FIG. 4: Different local mininima of the $Au_{11}/TiO_2(110)$ system in contact with a gas phase obtained by quenching configuration snapshots selected along the simulation.

manuscript. In the main manuscript we report the Löwdin charges of Au atoms solvated by water as a function of the simulation time, while the charge values of Fig. 3(a) have been obtained by first removing the solvent and then computing the Löwdin charges.

The same quenching protocol has been performed on selected configurations of $Au_{11}/TiO_2(110)$ in the corresponding gas phase situation. The Löwdin charges of Au atoms in the gas phase situation are plotted in the right panels (b) and (d) of Fig. 3 before and after the quenching. As depicted in the left panel of Fig. 3, in the case of the $Au_{11}/TiO_2(110)$ substrates isolated from the combined solid-liquid interface after the quenching each Au atoms of the nanocluster stabilizes its charge state which is the same for all the quenched snapshots. Thus, no change in the Löwdin charges is observed in all the selected snapshots. Namely, the simulated annealing found always the same local minimum. However, in the case of the $Au_{11}/TiO_2(110)$ catalyst in the gas phase situation we found several local minima. In Fig. 4, we show a set of different local minima sampled by the system. Here the

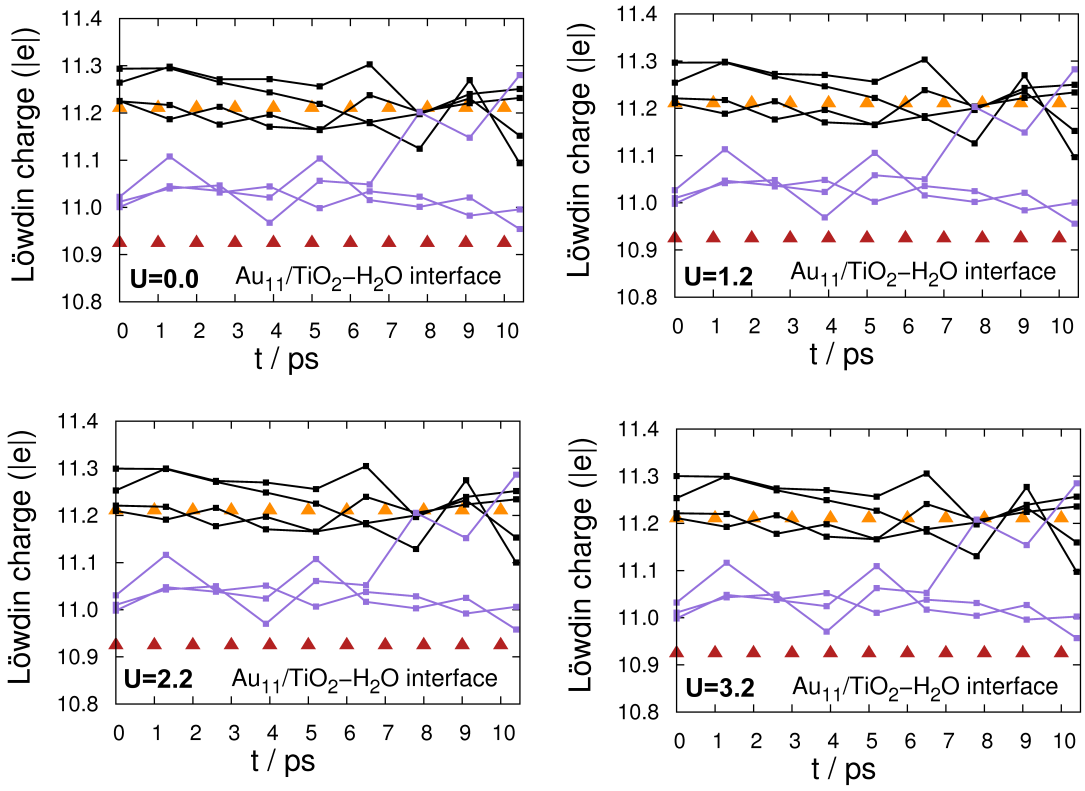

FIG. 5: Time evolution of the Löwdin charges of the top (violet lines) and middle (black lines) Au atoms of the supported gold nanocluster in liquid water at four different U values as indicated (0.0, 1.2, 2.2 and 3.2 eV); note that U =4.2 eV as determined and tested earlier [12, 13] has been used in the main study. Red and orange triangles correspond to reference Löwdin charges computed for a single Au^{+}(aq) cation (10.924 $|e|$) and Au^{0}(aq) atom (11.210 $|e|$) in liquid water, respectively.

various structures obtained differ in the charge values of the Au atoms, see right panel of Fig. 3.

Finally, we have carefully checked the charge distribution dependence on U by re-computing the Löwdin charges of the top and middle Au atoms of the supported gold nanocluster in liquid water for selected snapshots along the trajectory shown in Fig. 1(b) of the manuscript using four different U values (0.0, 1.2, 2.2 and 3.2 eV). The value U = 4.2 eV as used in the main study has been determined using the self–consistent linear response formalism [14, 15] and tested earlier in Refs. [12, 13]. As demonstrated by Fig. 5 the charge distribution is rather insensitive to U and thus does not show any significant dependence on the U value employed; see Ref. [1] for a thorough discussion of the impact of the Hubbard correction in the context of (defective) titania supports.

[1] P. M. Kowalski, B. Meyer, and D. Marx, Phys. Rev. B **79**, 115410 (2009).

[2] J. P. Perdew, K. Burke, and M. Ernzerhof, Phys. Rev. Lett. **77**, 3865 (1996); Phys. Rev. Lett. **78**, 1396(E) (1997).

[3] D. Vanderbilt, Phys. Rev. B **41**, 7892 (1990).

[4] A. C. Papageorgious *et al.*, PNAS **107**, 2391 (2010).

[5] E. Finazzi, C. Di Valentin, G. Pacchioni and A. Selloni, J. Chem. Phys. **129**, 154113 (2008).

[6] B. J. Morgan and G. W. Watson, J. Phys. Chem. C **113**, 7322 (2009).

[7] B. J. Morgan and G. W. Watson, Surf. Sci. **601**, 5034 (2007).

[8] F. Filipone, G. Mattioli, P. Alippi, and A. Amore Bonapasta, Phys. Rev. B **80**, 245203 (2009).

[9] C. J. Calzado, N. C. Hernández, and J. F. Sanz, Phys. Rev. B **77**, 045118 (2008).

[10] N. A. Deskins and M. Dupuis, Phys. Rev. B **75**, 195212 (2007).

[11] N. A. Deskins, R. Rousseau, and M. Dupuis, J. Phys. Chem. C **113**, 14583 (2009).

[12] P. M. Kowalski, M. Farnesi Camellone, N. N. Nair, B. Meyer, and D. Marx, Phys. Rev. Lett. **105**, 146405 (2010).

[13] M. Farnesi Camellone, P. M. Kowalski, and D. Marx, Phys. Rev. B **84**, 035413 (2011).

[14] M. Cococcioni and S. de Gironcoli, Phys. Rev. B **71**, 035105 (2005).

[15] H. J. Kulik, M. Cococcioni, D. A. Scherlis, and N. Marzari, Phys. Rev. Lett. **97**, 103001 (2006).

[16] P. Giannozzi *et al.*, J. Phys.: Condens. Matter **21**, 395502 (2009); `Quantum Espresso`, www.pwscf.org.

[17] D. Marx and J. Hutter, *Ab Initio Molecular Dynamics: Basic Theory and Advanced Methods* (Cambridge University Press, Cambridge 2009).

[18] R. Car and M. Parrinello, Phys. Rev. Lett. **55**, 2471 (1985).

[19] J. Hutter *et al.*, `CPMD`, www.cpmd.org.